Title

Pharmaceutical SH2 domain—containing protein tyrosine phosphatase 2 inhibition suppresses primary and metastasized liver tumors by provoking hepatic innate immunity

Journal

Hepatology, 77(5)

ISSN

0270-9139

Authors

Liu, Jacey J

Xin, Bing

Du, Li

et al.

Publication Date

2023-05-01

DOI

10.1002/hep.32555

Peer reviewed

HHS Public Access

Author manuscript

Hepatology. Author manuscript; available in PMC 2023 May 01.

Published in final edited form as:

Hepatology. 2023 May 01; 77(5): 1512–1526. doi:10.1002/hep.32555.

Pharmaceutical SH2 domain–containing protein tyrosine phosphatase 2 inhibition suppresses primary and metastasized liver tumors by provoking hepatic innate immunity

Jacey J. Liu[1], **Bing Xin**[2], **Li Du**[2], **Lydia Chen**[1], **Yanyan Long**[2], **Gen-Sheng Feng**[1,2]

[1]Department of Molecular Biology, School of Biological Sciences, University of California at San Diego, La Jolla, California, USA

[2]Department of Pathology and Moores Cancer Center, School of Medicine, University of California at San Diego, La Jolla, California, USA

Abstract

Background and Aims: SH2 domain–containing protein tyrosine phosphatase 2 (Shp2) is the first identified pro-oncogenic tyrosine phosphatase that acts downstream of receptor tyrosine kinases (RTKs) to promote Ras–extracellular signal–regulated kinase signaling. However, this phosphatase was also shown to be antitumorigenic in HCC. This study is aimed at deciphering paradoxical Shp2 functions and mechanisms in hepatocarcinogenesis and at exploring its value as a pharmaceutical target in HCC therapy.

Approaches and Results: We took both genetic and pharmaceutical approaches to examine the effects of Shp2 inhibition on primary liver cancers driven by various oncogenes and on metastasized liver tumors. We show here that the catalytic activity of Shp2 was essential for relay of oncogenic signals from RTKs in HCC and that chemical inhibition of Shp2 robustly suppressed HCC driven by RTKs. However, in contrast to a tumor-promoting hepatic niche generated by genetically deleting Shp2 in hepatocytes, treatment with a specific Shp2 inhibitor had a tumor-suppressing effect on metastasized liver tumor progression. Mechanistically, the Shp2 inhibitor enhanced antitumor innate immunity by down-regulating inflammatory cytokines, suppressing the chemokine (C-C motif) receptor 5 signaling axis, but up-regulating interferon-β secretion.

Conclusions: These results unveil complex mechanisms for the tumor-suppressing effect of pharmaceutical Shp2 inhibition in the liver immune environment. We provide a proof of principle for clinical trials with specific Shp2 inhibitors in patients with primary and metastasized liver cancer.

Correspondence: Gen-Sheng Feng, Department of Pathology, University of California at San Diego, Biomedical Research Facility II, 9500 Gilman Drive, Room 1220, La Jolla, CA 92093, USA. gfeng@health.ucsd.edu.

AUTHOR CONTRIBUTIONS

Gen-Sheng Feng and Jacey J. Liu conceived the project. Gen-Sheng Feng supervised all aspects of the experiments and the manuscript. Jacey J. Liu and Bing Xin designed and performed functional experiments and analyzed and interpreted data. Gen-Sheng Feng and Jacey J. Liu wrote the manuscript. Li Du, Lydia Chen, and Yanyan Long performed functional experiments and data analysis. Jacey J. Liu, Bing Xin, Li Du, Lydia Chen, Yanyan Long, and Gen-Sheng Feng reviewed the manuscript and provided input.

CONFLICT OF INTEREST

Nothing to report.

SUPPORTING INFORMATION

Additional supporting information may be found in the online version of the article at the publisher's website.

INTRODUCTION

HCC, the dominant type of liver cancer, is the seventh most frequently occurring cancer and a main cause of cancer-related mortality.[1] HCC has increasingly high incidence rates but is often diagnosed at late stages, excluding surgical resection and liver transplantation as treatment options.[2] More efficacious mechanism-based treatment is urgently needed, which requires comprehensive understanding of the molecular mechanisms in HCC pathogenesis. The Met axis plays a pivotal role in liver tumor development and metastasis; overexpression of Met or Met-dependent signature genes is frequently detected in HCC samples[3] and is associated with poor prognosis.[4–6] Consistently, overexpressing Met efficiently drove HCC development in transgenic mice,[7] but ablating Met in hepatocytes also exacerbated HCC development induced by the chemical carcinogen diethylnitrosamine (DEN) in mice,[8] suggesting complex tumorigenic mechanisms in the liver.

Cytoplasmic SH2 domain–containing protein tyrosine phosphatase 2 (Shp2; also known as protein tyrosine phosphatase nonreceptor type 11) is known to positively regulate cell growth and survival, mainly by promoting signaling from receptor tyrosine kinases (RTKs) to the Ras/extracellular signal–regulated kinase (Erk) pathway.[9] We showed that selectively deleting Shp2 in hepatocytes ($Shp2^{hep-/-}$) suppressed hepatocyte proliferation in liver regeneration and Erk activation by HGF and other growth factors.[10] HCC formation driven by two pairs of oncogenes, Met and β-catenin (Met/Cat) or Met and phosphatidylinositol-4,5-bisphosphate 3-kinase catalytic subunit alpha (PIK3CA; Met/Pik), was abolished in $Shp2^{hep-/-}$ mice, suggesting a critical role of Shp2 in Met-delivered oncogenic signaling.[11] However, the $Shp2^{hep-/-}$ mice also exhibited chronic hepatic damage, fibrosis, necrosis, and inflammation, resulting in aggravated HCC progression driven by DEN.[12] Concurrent deletion of Shp2 and phosphatase and tensin homolog perpetuated a severe phenotype of NASH-associated HCC,[13] and simultaneous removal of Shp2 and inhibitor of NF-κB kinase subunit beta even induced spontaneous HCC development by causing circadian disorders.[14] Thus, the Shp2 functions appear to be pleiotropic with both pro-oncogenic and antioncogenic effects, depending on the cellular context and the liver microenvironment, which are yet to be elucidated.

Interestingly, Shp2 is currently an extremely hot drug target in the pharmaceutical industry for oncological treatment, following development of an allosteric Shp2 inhibitor, SHP099, that robustly suppressed proliferation of tumor cells driven by oncogenic RTK signals.[15] This and similar compounds have been shown to effectively suppress tumor growth in various types of cancer, including lung cancer,[16] gastrointestinal cancer,[17] breast cancer,[18] and neuroblastoma[19]; and clinical trials are ongoing. However, the Shp2 inhibitor has not been tested in liver cancer in animal models in preclinical trials. Although the multifaceted roles of Shp2 raised caution on targeting Shp2 in HCC therapy,[20] it is hard to predict therapeutic efficacy of Shp2 inhibition based on cell type–specific gene deletion data. The outcome of clinical treatment relies collectively on the pharmaceutical effects of a drug in tumor cells as well as other cell types, especially immune cells, in the tumor microenvironment.

We took both genetic and pharmaceutical approaches to dissect Shp2 functions and mechanisms in hepatocarcinogenesis and to explore the therapeutic value of targeting Shp2 in primary and metastasized liver tumors. Unlike hepatocyte-specific Shp2 deletion that triggered hepatic damage and inflammation, pharmaceutical inhibition of Shp2 ameliorated inflammation in the tumor microenvironment, down-regulated the chemokine (C-C motif) receptor 5 (CCR5) signaling axis, and augmented interferon-β (IFNβ) secretion by hepatic macrophages, collectively leading to tumor suppression in the liver. This study reveals two separate mechanisms for the antitumor effect of Shp2 inactivation, a direct inhibitory effect of Shp2 on tumor cell proliferation and a modulatory effect of innate immune cells, which are of high clinical significance.

MATERIALS AND METHODS

Experimental mice and cell lines

The *Shp2*$^{hep-/-}$ (*Shp2*$^{fl/fl}$;*Alb-Cre*) mouse line in a C57BL/6 background was generated by breeding *Shp2*$^{fl/fl}$ mouse with albumin promoter-driven Cre recombinase transgenic mice, as described.[10,12] All animal studies were conducted on male *Shp2*$^{fl/fl}$ (wild type [WT]) or *Shp2*$^{fl/fl}$;*Alb-Cre* (*Shp2*$^{hep-/-}$) mice at age 6–23 weeks. Mice were group-housed (2–5 mice per cage) except that <5% of mice were singly housed at a later time period due to death of cage-mates. All mice were maintained under a 12-h light/dark cycle with free access to water and standard mouse chow food. All animals used in the study received humane care according to the criteria outlined in the Guide for the Care and Use of Laboratory Animals by NIH. The animal protocol (S09108) and the experimental procedures were approved by the Institutional Animal Care and Use Committee of University of California San Diego. MC38 colorectal cancer cells were a gift from the Karin Lab at University of California San Diego. HEK293T cells were obtained from the ATCC (CRL-3216; Manassas, VA).

Mouse tumor models and treatments

For primary liver cancer, oncogene-expressing DNA constructs were delivered by hydrodynamic tail vein injection into mice at 6–8 weeks of age to generate liver tumors, as described.[21] For metastasized liver tumors, mice were put under anesthesia and shaved at the left subcostal area. A left subcostal incision in line with the left ear was made through the skin and peritoneum. Then, the inferior half of the spleen was exposed through the incision, and MC38 tumor cells in PBS solution (100 μl) were injected through the inferior end of the spleen over a time period of 1–2 min. In the pharmaceutical treatment, SHP099 (Chemietek, Indianapolis, IN), trametinib (GSK1120212; APExBIO, Houston, TX), and Maraviroc (UK-427857; AdooQ Bioscience, Irvine, CA, USA) were dissolved in DMSO to make stock solutions at 100, 10, and 90 mg/ml. SHP099 was further diluted (1:24) in Ringer's solution, trametinib was diluted (1:29) in Ringer's solution, and Maraviroc was diluted in olive oil (1:8) as delivery vehicle. All three molecules were delivered by i.p. injection. Detailed experimental procedures are provided in the Supporting Information. We followed standard protocols to perform immunoblotting, immunostaining, RNA extraction, real-time quantitative PCR analysis, ELISA, and flow cytometry as well as cell culture.

Statistical analysis

Statistical analysis was done using GraphPad Prism 9. Statistical significance between means was calculated by the Student *t* test if not specified otherwise. Experiments that involved two independent variables placing influence on a dependent variable were statistically analyzed by two-way ANOVA together with multiple comparisons by the two-stage linear step-up procedure of Benjamini, Krieger and Yekutieli.

RESULTS

Shp2 is stringently required for hepatocarcinogenesis driven by RTK signaling

In previous experiments, we unveiled a critical role of Shp2 in the relay of oncogenic signals in liver tumorigenesis,[11] by hydrodynamic tail vein injection of oncogene-expressing constructs together with a sleeping beauty transposase.[21] Genetically deleting Shp2 in hepatocytes in mice (*Shp2*$^{fl/fl}$;*Alb-Cre*, *Shp2*$^{hep-/-}$) robustly suppressed HCC development driven by Met combined with a dominant active mutant of Cat (ΔCat; combination termed *Met/Cat*). Similarly, codelivery of Met/Pik, Met in combination with a hyperactive mutant of phosphoinositide 3-kinase (PI3K), p110α H1047R (PIK3CA^{HR}), did not efficiently induce liver tumors in *Shp2*$^{hep-/-}$ mice. We reasoned that Shp2 removal disrupted the transduction of oncogenic signals that emanated from Met, the RTK shared in the two oncogene pairs, Met/Cat and Met/Pik. To test this theory, we examined the tumorigenic effect of ΔCat and PIK3CA^{HR} (Cat/Pik), without Met included. We detected similar tumor burdens induced by Cat/Pik in *Shp2*$^{hep-/-}$ and WT livers (Figure 1A). Consistently, comparable levels of glutamine synthetase (GS) and phosphorylated Akt and Erk (pAkt and pErk) were detected in mutant and WT liver sections or lysates (Figures 1B and S1A). Lipid droplet accumulation, driven by overactivation of the PI3K pathway, was also similar in transfected WT and mutant livers (Figure S1C). Together, these results suggest that Shp2 is indeed necessary for the relay of oncogenic signals from Met but is dispensable for hepato-oncogenesis driven by Cat and PI3K mutants.

We also examined the impact of Shp2 deficiency on HCC driven by another pair of oncogenes, Nras^{G12V} and ΔCat (Ras/Cat). Notably, Shp2 deletion in hepatocytes did not impair but even aggravated Ras/Cat-driven tumors (Figure 1C,D), consistent with previous data showing a more severe tumor phenotype induced by DEN in *Shp2*$^{hep-/-}$ mice.[12] Likewise, cotransfection of Nras^{G12V} and a nuclear oncogene, c-Myc (Ras/Myc), caused heavier tumor loads in *Shp2*$^{hep-/-}$ than WT livers (Figure S1D). Augmented cell proliferation and more aggressive tumor progression were detected, as evaluated by Ki67 and cluster of differentiation 133 (CD133) levels in *Shp2*$^{hep-/-}$ versus WT livers following Ras/Myc transfection (Figures 1E and S1F).

To extend these observations in primary liver cancer, we evaluated the impact on metastasized liver tumors following intrasplenic injection of MC38 colorectal cancer cells. Indeed, more aggressive growth of metastasized tumors was observed in *Shp2*$^{hep-/-}$ than WT livers (Figure 1F). In aggregate, these experiments, while disclosing a cell-intrinsic role of Shp2 in RTK-driven hepatocarcinogenesis, also reveal that genetic ablation of Shp2 in

hepatocytes induced formation of a hepatic microenvironment conducive for growth of both primary and metastasized tumors.

Catalytic activity is essential for Shp2 relay of oncogenic signals from RTKs

To decipher the biochemical mechanism underlying a pivotal role of Shp2 in RTK-dependent tumorigenesis, we performed cotransfection of $Shp2^{WT}$, $Shp2^{CS}$ (catalytically inactive C463S mutant), or $Shp2^{DA}$ (constitutively active mutant) with Met/Cat or Met/Pik oncogenes. Codelivery of $Shp2^{WT}$ or $Shp2^{DA}$ mutant rescued the tumor phenotype in $Shp2^{hep-/-}$ mice induced by the two oncogene pairs, but the $Shp2^{CS}$ mutant failed to do so (Figures 2A and S2A,C,I). Furthermore, cotransfection of the $Shp2^{CS}$ mutant even suppressed Met/Cat-induced tumors in WT mice (Figures 2A and S2B). These results indicate a stringent requirement for Shp2 catalytic activity in Met-driven oncogenic signaling in hepatocytes. Consistent with the rescued tumor phenotype, reexpressing $Shp2^{WT}$ in Shp2-deficient hepatocytes restored Met-mediated and Cat-mediated signaling events and restored ectopic expression of Met, which was not stably expressed in Shp2-deficient hepatocytes (Figures 2B and S2D). Expressing the $Shp2^{CS}$ mutant resulted in hepatocyte senescence (Figure 2C), contributing to tumor suppression in WT liver (Figure 2A).

Because suppressor of cytokine signaling 1 (Socs1) was shown to inhibit Met expression and signaling,[22] we explored a putative role of Socs1 in mediating Shp2 modulation of Met activity. Expressing a dominant-negative mutant of Socs1 ($Socs1^{F59D}$) partially restored Met/Cat-induced tumor phenotype in $Shp2^{hep-/-}$ liver (Figure 2D). Meanwhile, introducing a dominant-negative mutant of Socs3 ($Socs3^{F25A}$), another member of the family, drove a more severe tumor phenotype (Figure 2D). However, cotransfection of $Socs3^{F25A}$ mutant with ΔCat, without including Met, did not induce tumor formation in $Shp2^{hep-/-}$ liver (Figure S2F), suggesting that abrogating the Socs1 or Socs3 function plays a permissive role in Met signaling but is not sufficient to drive HCC. The impaired Met expression in Shp2-deficient hepatocytes was rescued by cotransfection with $Socs3^{F25A}$ mutant (Figures 2E and S2J). More aggressive tumor progression and higher CD133 expression were observed following expression of an undegradable mutant, Met^{Y1003F} (Met^{YF}), with abundant Met protein detected on the cell surface (Figures 2F and S2D,G,H). Together, these results suggest that Shp2 promoted oncogenic signaling of RTKs at least in part by overcoming Socs3-mediated down-regulation of Met expression and activity.

Pharmaceutical inhibition of Shp2 robustly suppresses primary liver cancer

Given the paradoxical tumor-suppressing and tumor-promoting effects of Shp2 deficiency in cell-intrinsic oncogenic signaling and the tumor microenvironment, we wanted to determine how an Shp2 inhibitor might influence HCC progression. First, we examined the effect of an allosteric Shp2 inhibitor (SHP099) in cultured HEK293T cells *in vitro*. As expected, SHP099 inhibited pErk signal stimulated by Met overexpression and HGF, the Met ligand (Figure S3A,C); but SHP099 failed to inhibit Ras-induced pErk signal in Ras/Myc-transfected cells (Figure S3B). Next, we tested its therapeutic effect in mouse HCC driven by Met/Cat. At approximately Week 7 after oncogene transfection when tumor nodules reached 2–3 mm, SHP099 was administrated to tumor-bearing mice i.p. every day

for 3 weeks. SHP099 treatment effectively decreased tumor sizes and numbers compared to vehicle control (Figure 3A). Shp2 inhibition impaired pErk activation and hampered proliferation of Met^+ tumor cells (Figures 3B,C and S3D). These results demonstrate a therapeutic effect of SHP099 in an autochthonous HCC model, although the treatment did not cause a complete tumor remission.

We further tested the therapeutic effect of SHP099 in HCC driven by Ras/Myc. The Shp2 inhibitor exhibited no significant suppression on tumor progression, tumor cell proliferation, and pErk signals (Figures 3D–F and S3E). However, treatment with trametinib, a Mek inhibitor, showed a robust suppression of Ras/Myc-driven tumor progression (Figure 3D). The poor efficacy of SHP099 in this tumor model was expected because Shp2 was dispensable for Ras/Myc-driven HCC, as revealed by genetic manipulation (Figure S1D).

Pharmaceutical inactivation of Shp2 prevents metastasized tumor growth in the liver

We wondered if chemical inhibition of Shp2 also induced a protumorigenic niche in the liver, similar to genetic removal of Shp2 from hepatocytes (Figure 1F). To address this issue, we pretreated WT mice with SHP099 before splenic injection of MC38 tumor cells. In contrast to genetic ablation of Shp2, pretreatment with SHP099 suppressed growth of metastasized tumors in the liver (Figure 4A). The tumor-inhibitory effect of SHP099 pretreatment gradually diminished, as revealed by implanting tumor cells at Day 3 or 10 following the last injection of the compound (Figure S4A). However, pretreatment with trametinib did not exhibit a similar inhibitory effect on metastasized tumors (Figure S4B), suggesting a unique hepatoprotective effect of pharmaceutical Shp2 inhibition. We investigated the distinct effects of chemical inhibition and genetic ablation of Shp2 in remodeling the liver microenvironment. Hepatic inflammation was induced in $Shp2^{hep-/-}$ mice, featured by inflammatory immune cell accumulation near portal triads and ballooning hepatocytes (Figure 4B). However, SHP099-treated livers exhibited normal and healthy histology (Figure 4B). Liver fibrosis and enlarged gallbladder induced in $Shp2^{hep-/-}$ mice were not observed in SHP099-treated mice (Figures 4C and S4C).

We compared the effects of gene deletion and chemical inhibition on hepatic immune cell profiles. Flow cytometry showed that neither perturbation significantly altered the percentages of T, B, natural killer (NK) T, and NK cells in the $CD45^+$ cell population (Figure S5A). However, the absolute numbers of most immune cell subsets increased significantly in $Shp2^{hep-/-}$ livers, which were undermined by SHP099 treatment (Figures 4D and S5I), in agreement with the histological observation of increased immune cell infiltration. The absolute numbers, but not percentages, of proliferative and activated T cells and NK cells tended to increase in $Shp2^{hep-/-}$ liver (Figure S6A–E). Programmed death ligand 1 (PD-L1) expression on macrophages and LSECs was up-regulated (Figure S6F). Moreover, Shp2 deletion favored M1 polarization of macrophages, another sign of enhanced inflammatory response in $Shp2^{hep-/-}$ liver (Figure 4E). In comparison to genetic deletion, treatment with SHP099 caused only modest alterations in immune cell profiles in WT mice and partially offset the composition changes of immune cell subsets in $Shp2^{hep-/-}$ livers (Figures 4D,E and S5A–F). Thus, pharmaceutical Shp2 inhibition did not phenocopy the hepato-damaging phenotype of Shp2 deletion but rather exhibited a hepatoprotective effect.

Shp2 inactivation has multiple effects on the tumor immune environment

Because the analysis above suggests a potential role of SHP099 in improving the hepatic immune landscape, we further examined how the inhibitor pretreatment influenced hepatic immune cells under the stress of metastasized tumor progression. SHP099 down-regulated $CD3^+$ T cell percentages in $CD45^+$ cells, while leaving $CD4^+$, $CD8^+$ T cell ratios unchanged (Figure S7A,C). The percentages of proliferative $CD4^+$, $CD8^+$ T cells and NK cells were up-regulated by SHP099 pretreatment, especially at early stages of tumor metastasis (Figure 5A), while ratios of activated cells in these subsets remained similar to the control (Figure S7D–F). The regulatory T cell (Treg) percentages were increased (Figure 5B), and the $CD8^+/CD4^+$ T cell and $CD8^+$/Treg ratios were not altered by SHP099 pretreatment (Figure S7G,H).

In the hepatic myeloid compartment, SHP099 pretreatment up-regulated the percentages of $CD11b^+$ cells and dendritic cells but down-regulated macrophage percentages, without significant impact on the percentages of resident Kupffer cells, which comprise the majority of hepatic macrophages (Figure S8A–E). Conventional macrophage polarization was marginally affected by SHP099 (Figure 5C). Interestingly, M1 and M2a polarized macrophages comprised only a minor portion, while M2b macrophages ($F4/80^+$ $CD11c^-$ major histocompatibility complex II–positive [$MHCII^+$]) comprised the majority of hepatic macrophages (Figure 5C), which is an alternatively polarized macrophage group with proinflammatory and tumor-promoting activities.[23]

Given a decrease in M2b polarized Kupffer cell ratios by SHP099 (Figure S8F), we evaluated whether the M2b-associated proinflammatory response was also affected by the compound. On Days 7 and 9 post–tumor cell inoculation, SHP099 pretreatment down-regulated expression of proinflammatory factors IL-1β, IL-6, and TNFα (Figure 5D), as well as the M2b macrophage polarization marker LIGHT/TNFSF14 (Figure 5E), suggesting that SHP099 reduced inflammatory responses that could aggravate metastasized tumor progression. By measuring a full panel of C-C motif and C-X-C motif chemokine ligands, we detected a significant drop in chemokine (C-C motif) ligand 4 (CCL4) and CCL5 expression in SHP099-pretreated livers (Figures 5F and S9). Consistently, the expression of their corresponding receptors CCR2 and CCR5 was also down-regulated, accompanied by lower expression of IFN regulatory factor 5 (IRF5), a master regulator for inflammatory response and CCL5 expression (Figure 5F). Because the CCL4/5–CCR2/5 axis and IRF5 are known to promote inflammation,[24,25] their reduced expression suggests that SHP099 ameliorated hepatic inflammation, leading to less severe tumor development. In contrast to SHP099 pretreatment, CCL5–CCR5 axis–related genes were up-regulated by genetic Shp2 deletion in hepatocytes (Figure 4F), revealing an association of the CCL5–CCR5 axis, inflammation, and tumor progression. Together, these results unveil opposite environmental impacts, especially the bidirectional regulation of CCL5–CCR5 signaling, induced by genetic deletion of Shp2 in hepatocytes and chemical inhibition of Shp2, leading to the protumorigenic and antitumorigenic effects. Unlike its effect in the liver, systemic treatment with SHP099 did not suppress MC38 tumor cell growth in the spleen (Figure S12A) and did not influence immune cell ratios and the tumor microenvironmental factors (Figure S12B–E).

Shp2 inhibition enhances IFNβ secretion from liver macrophages

CCR5 was most abundantly expressed in liver macrophages as measured by flow cytometry, with nearly 43% of macrophages being CCR5-positive (Figure 6A). The second group was LSECs at 23%, followed by $CD8^+$ T cells at 16.8%, among the nonparenchymal cell types examined (Figures 6A and S10A). Largely overlapping cell surface expression of F4/80 and CCR5 supported the CCR5 abundance on liver macrophages (Figure 6E). These data suggest a critical role of CCL5–CCR5 signaling in modulating macrophage functions, consistent with a previous report on CCL5-mediated augmentation of tumor-associated macrophage (TAM) function.[26] This study also showed that CCR5 inhibition could lead to TAM repolarization and stimulate IFN production in macrophages.[26] We detected drastically increased expression of IFNα1, IFNα2, and IFNβ1, as well as increased expression and phosphorylation of IRF3, a transcription factor for type I IFNs in SHP099-pretreated liver (Figure 6B,C). Consistently, we observed significantly up-regulated IFNβ secretion from isolated liver macrophages following SHP099 treatment *in vitro* (Figure 6D) but not from isolated dendritic cells (Figure S10B), identifying macrophages as the main source of IFNβ. These results suggest that Shp2 inhibition enhanced IFNβ secretion from macrophages and ameliorated inflammation through suppressing CCR5 signaling, generating an antitumor niche in the liver. Treatment with a CCR5 antagonist, Maraviroc, also promoted IFNα and IFNβ expression (Figure 7A) but did not stimulate IFNβ secretion from isolated macrophages (Figure 6D) or up-regulate phosphorylation of IRF3 *in vivo* (Figure S10E), suggesting that suppressed CCR5 signaling and augmented IFNβ secretion from macrophages are two separate events induced by SHP099 pretreatment.

Maraviroc treatment did not effectively inhibit metastasized tumor growth in the liver (Figure 7B), likely because of its failure to alleviate severe inflammation in the tumor microenvironment and to cap the compensatory up-regulation of CCL5–CCR5 axis gene expression (Figures 7C and S10C). SHP099 pretreatment reduced cell surface CCR5 level and restricted CCR5 expression to intracellular discrete puncta in macrophages (Figure 6E,F), whereas in control and Maraviroc-treated liver, CCR5 was mostly dispersed in the cytoplasm (Figure S10D). Thus, Shp2 inhibition retained at least part of CCR5 in intracellular puncta of macrophages to hinder their recycling back to cell membrane. We also demonstrated that following splenic injection of MC38 cells, SHP099 treatment significantly suppressed metastasized tumor progression in the liver (Figure 7D). This result further suggests a therapeutic effect of SHP099, through acting on both tumor cells and hepatic niche cells. Mechanistically, SHP099 attenuated the oncogenic ERK pathway in malignant cells, suppressed the CCR5 axis, and enhanced IFNβ secretion from hepatic macrophages.

DISCUSSION

In this study, we obtained consistent data from genetic perturbation and pharmaceutical inhibition which indicate a stringent requirement of Shp2's catalytic activity for oncogenic signaling in hepatocytes driven by Met. However, these two experimental approaches gave rise to interestingly different results with regard to the impact of Shp2 deficiency on the hepatic microenvironment, especially the innate immune cell functions, associated

with liver tumor progression. Our previous experiments showed that deleting Shp2 in hepatocytes suppressed development of autochthonous liver tumors driven by Met and Cat,[11] although the underlying molecular mechanism was unclear. In extending the previous observation, this study demonstrated that the catalytic activity of Shp2 was essential for the oncogenic signal relay. In interrogating the biochemical mechanism, we identified Socs3 as a molecule that counteracts Shp2 function in hepato-oncogenesis. Socs3 possesses an SH2 domain that shares similar binding specificity with Shp2[27–29] and thus possibly competes with Shp2 for Met binding. Following binding to target molecules, Socs3 can recruit ubiquitin ligase for ubiquitination and degradation of its targets.[30] Indeed, we observed that abrogating Socs3 function or expressing an undegradable Met mutant restored Met/Cat-induced tumor formation and steady Met expression in $Shp2^{hep-/-}$ liver (Figures 2D–F and S2D,G,J). In addition to its crucial cell-intrinsic function, genetic data unveiled a distinct cell-extrinsic Shp2 function. Deleting Shp2 in hepatocytes even aggravated Ras/Myc-driven primary tumor and metastasized tumor growth in the liver, by inducing a tumor-promoting microenvironment (Figures 1F and S1D,F). These results revealed an antioncogenic role of Shp2, which has also been observed in another study of oncogene-induced hepatocarcinogenesis.[31]

Great efforts are being devoted to advancing Shp2-targeted oncological treatment in the pharmaceutical industry. Recently, a series of allosteric Shp2 inhibitors including SHP099 showed therapeutic efficacy on a variety of RTK/Ras/Erk pathway–dependent cancer cell lines and animal tumor models, as either single or combined therapy with other kinase inhibitors targeting this pathway.[15–19] However, the paradoxical pro-oncogenic and antioncogenic effects of Shp2 in HCC raised a caution on inhibiting Shp2 in liver cancer treatment, and the tumor-promoting hepatic microenvironment formed in $Shp2^{hep-/-}$ mice would even argue against Shp2 as a pharmaceutical target. To address this concern, we carefully examined the effects of pharmaceutical Shp2 inhibition on primary and metastasized liver tumors. Consistent with the gene deletion data, SHP099 treatment significantly suppressed progression of Met/Cat-induced liver tumors, validating a critical role of Shp2 in the Met pathway (Figure 3A–C). Moreover, we found that chemical inhibition of Shp2 even exerted a tumor-suppressive effect on metastasized liver tumors (Figure 4A), opposite to the protumorigenic effect observed in $Shp2^{hep-/-}$ liver. Mechanistically, Shp2 deletion in hepatocytes led to increased immune cell infiltration, fibrosis, and cholestasis, constituting a tumor-promoting hepatic niche (Figure 4B–F). In contrast, pharmaceutical Shp2 inactivation remedied the inflammatory environment by controlling immune cell infiltration (Figure 4D) and reducing expression of proinflammatory cytokines (Figure 5D). It should be noted that direct comparison of the outcomes between genetic perturbation and pharmaceutical inhibition would be unfair because of variations in the durations of the effects and the cell types affected, and this point was reinforced by our mechanistic analysis of the Shp2 inhibitor's tumor-suppressive effects. We analyzed hepatic immune cell profiles, and only modest changes in adaptive immune cell subsets were observed in SHP099-treated liver (Figure S7A,C). There was a significant up-regulation of T cell and NK cell proliferation but not activation (Figures 5A and S7D–F), and it was accompanied by a compensatory up-regulation of Treg cell ratios (Figure 5B), resulting in an overall neutral effect on adaptive cell immunity by SHP099. Although Shp2 was reported

to interact with programmed death-1 in T cells and Shp2 deficiency was shown to enhance T cell–mediated antitumor immunity,[32,33] Shp2 inhibition did not significantly change the adaptive immune activity in the metastasized tumor-bearing livers, as revealed by unaltered PD-L1 levels and $CD8^+$ T/Treg ratios (Figures S6F and S7H).

These data prompted us to shift attention to potential roles of innate immune cells. Despite its marginal effect on myeloid cell composition (Figure S8), SHP099 treatment modulated Kupffer cell polarization and reduced M2b-polarized Kupffer cell ratios (Figures5E and S8F). M2b macrophages are known to be associated with inflammation and the tumor-promoting property.[23] Expression of components in the CCL5–CCR5 pathway, a critical regulatory axis in inflammation, was attenuated by SHP099, concomitant with impaired expression of proinflammatory factors in liver nonparenchymal cells (Figure 5D,F). Several groups reported that CCL5–CCR5 signaling promoted hepatic fibrosis[34] and inflammation-associated HCC.[35] We found that CCR5 was substantially expressed in macrophages (Figure 6A), suggesting that the CCR5 axis in macrophages is prone to be influenced by SHP099 treatment. Indeed, SHP099 treatment enhanced internalization and retention of CCR5 in subcellular perinuclear punctate structure in liver macrophages (Figure 6E), which hindered the activity of CCR5 signaling. Previous studies have also suggested a critical role of Shp2 in regulating macrophage polarization and inflammation-related secretory profiles.[36,37] In this study, we further specified M2b polarization and the CCR5 pathway being significantly modified by Shp2 inhibition, which contributed to alleviating the inflammation in the liver. CCR5 pathway stimulation leading to inflammation was reportedly dependent on the mitogen-activated protein kinase pathway,[38] through which Shp2 inhibition could impede the CCR5 signaling axis. Systemic delivery of SHP099 may influence functions of other immune organs such as the spleen. However, SHP099 treatment did not exhibit significant impact on T cell proliferation, proinflammatory responses, and the CCR5 pathway in the spleen, unlike that in liver (Figure S12B–E), with no significant suppression of splenic tumors derived from MC38 cells (Figure S12A). Together, these results suggested that SHP099 did not reshape a tumor microenvironment in the spleen as in the liver, which is likely attributable to low abundance of myeloid cells that can be targeted by SHP099 in the spleen.

Of note, we observed a significant effect of Type I IFN induction by SHP099, especially the up-regulated IFNβ secretion from macrophages (Figure 6D). Consistent with this observation, we showed previously that polyinosinic:polycytidylic acid, a potent IFN inducer, effectively prevented HCC initiation and suppressed tumor progression in combination with anti-PD-L1 antibody.[39–41] We believe that the tumor-suppressive role of the Shp2 inhibitor in the liver microenvironment is associated with multiple effects and mechanisms, including down-regulation of inflammatory cytokines, suppression of the CCR5 axis, and up-regulation of IFN signaling, which work in concert to enhance the hepatic antitumor innate immunity. More experiments are warranted to elucidate the complex molecular and cellular mechanisms and to further improve the efficacy, but this study has demonstrated an encouraging therapeutic benefit of targeting Shp2 in primary and metastasized liver tumors.

Supplementary Material

Refer to Web version on PubMed Central for supplementary material.

ACKNOWLEDGMENTS

We thank Dr. X. Chen (University of Hawaii) and Dr. J. Ohlfest for reagents. We also thank the University of California San Diego School of Medicine Microscopy Core (P30NS047101) and Tissue Technology Shared Resource (NIHP30CA23100). We are grateful to the University of California San Diego Human ES Cell Core Facility as well as C. Fine, M. Espinoza, and A. Rider (the University of California San Diego) for technical assistance with flow-cytometric experiments. This work was made possible by the University of California San Diego's Stem Cell Program and a California Institute for Regenerative Medicine Major Facilities grant (FA1–00607) to the Sanford Consortium for Regenerative Medicine. The graphical abstract was created with BioRender.com.

Funding information

National Institutes of Health, Grant/Award Number: R01CA236074, R01CA239629 and P01AG073084; Krueger v. Wyeth research award to G.S.F.

Abbreviations:

Alb-Cre	albumin promoter-driven Cre recombinase
Cat	β-catenin
CCL	chemokine (C-C motif) ligand
CCR	chemokine (C-C motif) receptor
CD	cluster of differentiation
DEN	diethylnitrosamine
ERK	extracellular signal–regulated kinase
GS	glutamine synthetase
IFN	interferon
IRF5	IFN regulatory factor 5
MHCII	major histocompatibility complex II
NK	natural killer
p-	phosphorylated
PD-L1	programmed death ligand 1
PI3K	phosphoinositide 3-kinase
PIK3CA/Pik	phosphatidylinositol-4,5-bisphosphate 3-kinase catalytic subunit alpha
RTK	receptor tyrosine kinase

Shp2	SH2 domain–containing protein tyrosine phosphatase 2
Shp2^{CS}	catalytically inactive C463S mutant
Socs1	suppressor of cytokine signaling 1
Treg	regulatory T cell
WT	wild type

REFERENCES

1. Bray F, Ferlay J, Soerjomataram I, Siegel RL, Torre LA, Jemal A. Global cancer statistics 2018: GLOBOCAN estimates of incidence and mortality worldwide for 36 cancers in 185 countries. CA Cancer J Clin 2018;68:394–424. [PubMed: 30207593]
2. Llovet JM, De Baere T, Kulik L, Haber PK, Greten TF, Meyer T, et al. Locoregional therapies in the era of molecular and immune treatments for hepatocellular carcinoma. Nat Rev Gastroenterol Hepatol 2021;18:293–313. [PubMed: 33510460]
3. Tavian D, De Petro G, Benetti A, Portolani N, Giulini SM, Barlati S. u-PA and c-MET mRNA expression is co-ordinately enhanced while hepatocyte growth factor mRNA is down-regulated in human hepatocellular carcinoma. Int J Cancer 2000;87:644–9. [PubMed: 10925356]
4. Osada S, Kanematsu M, Imai H, Goshima S. Clinical significance of serum HGF and c-Met expression in tumor tissue for evaluation of properties and treatment of hepatocellular carcinoma. Hepatogastroenterology 2008;55:544–9. [PubMed: 18613405]
5. Daveau M, Scotte M, Francois A, Coulouarn C, Ros G, Tallet Y, et al. Hepatocyte growth factor, transforming growth factor alpha, and their receptors as combined markers of prognosis in hepatocellular carcinoma. Mol Carcinog 2003;36:130–41. [PubMed: 12619035]
6. Kaposi-Novak P, Lee JS, Gomez-Quiroz L, Coulouarn C, Factor VM, Thorgeirsson SS. Met-regulated expression signature defines a subset of human hepatocellular carcinomas with poor prognosis and aggressive phenotype. J Clin Invest 2006;116:1582–95. [PubMed: 16710476]
7. Wang R, Ferrell LD, Faouzi S, Maher JJ, Bishop JM. Activation of the Met receptor by cell attachment induces and sustains hepatocellular carcinomas in transgenic mice. J Cell Biol 2001;153:1023–34. [PubMed: 11381087]
8. Marx-Stoelting P, Borowiak M, Knorpp T, Birchmeier C, Buchmann A, Schwarz M. Hepatocarcinogenesis in mice with a conditional knockout of the hepatocyte growth factor receptor c-Met. Int J Cancer 2009;124:1767–72. [PubMed: 19123478]
9. Chan RJ, Feng GS. PTPN11 is the first identified protooncogene that encodes a tyrosine phosphatase. Blood 2007;109:862–7. [PubMed: 17053061]
10. Bard-Chapeau EA, Yuan J, Droin N, Long S, Zhang EE, Nguyen TV, et al. Concerted functions of Gab1 and Shp2 in liver regeneration and hepatoprotection. Mol Cell Biol 2006;26:4664–74. [PubMed: 16738330]
11. Liu JJ, Li Y, Chen WS, Liang Y, Wang G, Zong M, et al. Shp2 deletion in hepatocytes suppresses hepatocarcinogenesis driven by oncogenic beta-Catenin, PIK3CA and MET. J Hepatol 2018;69:79–88. [PubMed: 29505847]
12. Bard-Chapeau E, Li S, Ding J, Zhang S, Zhu H, Princen F, et al. Ptpn11/Shp2 acts as a tumor suppressor in hepatocellular carcinogenesis. Cancer Cell 2011;19:629–39. [PubMed: 21575863]
13. Luo X, Liao R, Hanley KL, Zhu HH, Malo KN, Hernandez C, et al. Dual Shp2 and Pten deficiencies promote non-alcoholic steatohepatitis and genesis of liver tumor-initiating cells. Cell Rep 2016;17:2979–93. [PubMed: 27974211]
14. Hanley KL, Liang Y, Wang G, Lin X, Yang M, Karin M, et al. Concurrent disruption of the Ras/MAPK and NF-κB pathways induces circadian deregulation and hepatocarcinogenesis. Mol Cancer Res 2021. 10.1158/1541-7786.MCR-21-0479

15. Chen Y-N, LaMarche MJ, Chan HM, Fekkes P, Garcia-Fortanet J, Acker MG, et al. Allosteric inhibition of SHP2 phosphatase inhibits cancers driven by receptor tyrosine kinases. Nature 2016;535:148–52. [PubMed: 27362227]
16. Mainardi S, Mulero-Sánchez A, Prahallad A, Germano G, Bosma A, Krimpenfort P, et al. SHP2 is required for growth of KRAS-mutant non-small-cell lung cancer in vivo. Nat Med 2018;24:961–7. [PubMed: 29808006]
17. Wong GS, Zhou J, Liu JB, Wu Z, Xu X, Li T, et al. Targeting wildtype KRAS-amplified gastroesophageal cancer through combined MEK and SHP2 inhibition. Nat Med 2018;24:968–77. [PubMed: 29808010]
18. Ahmed TA, Adamopoulos C, Karoulia Z, Wu X, Sachidanandam R, Aaronson SA, et al. SHP2 drives adaptive resistance to ERK signaling inhibition in molecularly defined subsets of ERK-dependent tumors. Cell Rep 2019;26:65–78.e5. [PubMed: 30605687]
19. Valencia-Sama I, Ladumor Y, Kee L, Adderley T, Christopher G, Robinson CM, et al. NRAS status determines sensitivity to SHP2 inhibitor combination therapies targeting the RAS–MAPK pathway in neuroblastoma. Cancer Res 2020;80:3413–23. [PubMed: 32586982]
20. Li S, Hsu DD, Wang H, Feng GS. Dual faces of SH2-containing protein-tyrosine phosphatase Shp2/PTPN11 in tumorigenesis. Front Med 2012;6:275–9. [PubMed: 22869052]
21. Chen X, Calvisi DF. Hydrodynamic transfection for generation of novel mouse models for liver cancer research. Am J Pathol 2014;184:912–23. [PubMed: 24480331]
22. Gui Y, Yeganeh M, Donates Y-C, Tobelaim W-S, Chababi W, Mayhue M, et al. Regulation of MET receptor tyrosine kinase signaling by suppressor of cytokine signaling 1 in hepatocellular carcinoma. Oncogene 2015;34:5718–28. [PubMed: 25728680]
23. Wang LX, Zhang SX, Wu HJ, Rong XL, Guo J. M2b macrophage polarization and its roles in diseases. J Leukoc Biol 2019;106:345–58. [PubMed: 30576000]
24. Kitade H, Sawamoto K, Nagashimada M, Inoue H, Yamamoto Y, Sai Y, et al. CCR5 plays a critical role in obesity-induced adipose tissue inflammation and insulin resistance by regulating both macrophage recruitment and M1/M2 status. Diabetes 2012;61:1680–90. [PubMed: 22474027]
25. Weiss M, Byrne AJ, Blazek K, Saliba DG, Pease JE, Perocheau D, et al. IRF5 controls both acute and chronic inflammation. Proc Natl Acad Sci U S A 2015;112:11001–6. [PubMed: 26283380]
26. Halama N, Zoernig I, Berthel A, Kahlert C, Klupp F, Suarez-Carmona M, et al. Tumoral immune cell exploitation in colorectal cancer metastases can be targeted effectively by anti-CCR5 therapy in cancer patients. Cancer Cell 2016;29:587–601. [PubMed: 27070705]
27. Nicholson SE, De Souza D, Fabri LJ, Corbin J, Willson TA, Zhang J-G, et al. Suppressor of cytokine signaling-3 preferentially binds to the SHP-2-binding site on the shared cytokine receptor subunit gp130. Proc Natl Acad Sci U S A 2000;97:6493–8. [PubMed: 10829066]
28. Schmitz J, Weissenbach M, Haan S, Heinrich PC, Schaper F. SOCS3 exerts its inhibitory function on interleukin-6 signal transduction through the SHP2 recruitment site of gp130. J Biol Chem 2000;275:12848–56. [PubMed: 10777583]
29. Forrai A, Boyle K, Hart AH, Hartley L, Rakar S, Willson TA, et al. Absence of suppressor of cytokine signalling 3 reduces self-renewal and promotes differentiation in murine embryonic stem cells. Stem Cells 2006;24:604–14. [PubMed: 16123385]
30. Rui L, Yuan M, Frantz D, Shoelson S, White MF. SOCS-1 and SOCS-3 block insulin signaling by ubiquitin-mediated degradation of IRS1 and IRS2. J Biol Chem 2002;277:42394–8. [PubMed: 12228220]
31. Chen WS, Liang Y, Zong M, Liu JJ, Kaneko K, Hanley KL, et al. Single-cell transcriptomics reveals opposing roles of Shp2 in Myc-driven liver tumor cells and microenvironment. Cell Rep 2021;37:109974. [PubMed: 34758313]
32. Hui E, Cheung J, Zhu J, Su X, Taylor MJ, Wallweber HA, et al. T cell costimulatory receptor CD28 is a primary target for PD-1-mediated inhibition. Science 2017;355:1428–33. [PubMed: 28280247]
33. Wang B, Zhang W, Jankovic V, Golubov J, Poon P, Oswald EM, et al. Combination cancer immunotherapy targeting PD-1 and GITR can rescue CD8+ T cell dysfunction and maintain memory phenotype. Sci Immunol 2018;3:eaat7061. [PubMed: 30389797]

34. Seki E, De Minicis S, Gwak G-Y, Kluwe J, Inokuchi S, Bursill CA, et al. CCR1 and CCR5 promote hepatic fibrosis in mice. J Clin Invest 2009;119:1858–70. [PubMed: 19603542]

35. Barashi N, Weiss ID, Wald O, Wald H, Beider K, Abraham M, et al. Inflammation-induced hepatocellular carcinoma is dependent on CCR5 in mice. Hepatology 2013;58:1021–30. [PubMed: 23526353]

36. Xiao P, Zhang H, Zhang YU, Zheng M, Liu R, Zhao Y, et al. Phosphatase Shp2 exacerbates intestinal inflammation by disrupting macrophage responsiveness to interleukin-10. J Exp Med 2019;216:337–49. [PubMed: 30610104]

37. Wang S, Yao Y, Li H, Zheng G, Lu S, Chen W. Tumor-associated macrophages (TAMs) depend on Shp2 for their anti-tumor roles in colorectal cancer. Am J Cancer Res 2019;9:1957–69. [PubMed: 31598397]

38. Li M, Sun X, Zhao J, Xia L, Li J, Xu M, et al. CCL5 deficiency promotes liver repair by improving inflammation resolution and liver regeneration through M2 macrophage polarization. Cell Mol Immunol 2020;17:753–64. [PubMed: 31481754]

39. Lee J, Liao R, Wang G, Yang B-H, Luo X, Varki NM, et al. Preventive inhibition of liver tumorigenesis by systemic activation of innate immune functions. Cell Rep 2017;21:1870–82. [PubMed: 29141219]

40. Wen L, Xin B, Wu P, Lin C-H, Peng C, Wang G, et al. An efficient combination immunotherapy for primary liver cancer by harmonized activation of innate and adaptive immunity in mice. Hepatology 2019;69:2518–32. [PubMed: 30693544]

41. Xin B, Yang M, Wu P, Du L, Deng X, Hui E, et al. Enhancing the therapeutic efficacy of programmed death ligand 1 antibody for metastasized liver cancer by overcoming hepatic immuno-tolerance in mice. Hepatology 2021. 10.1002/hep.32266

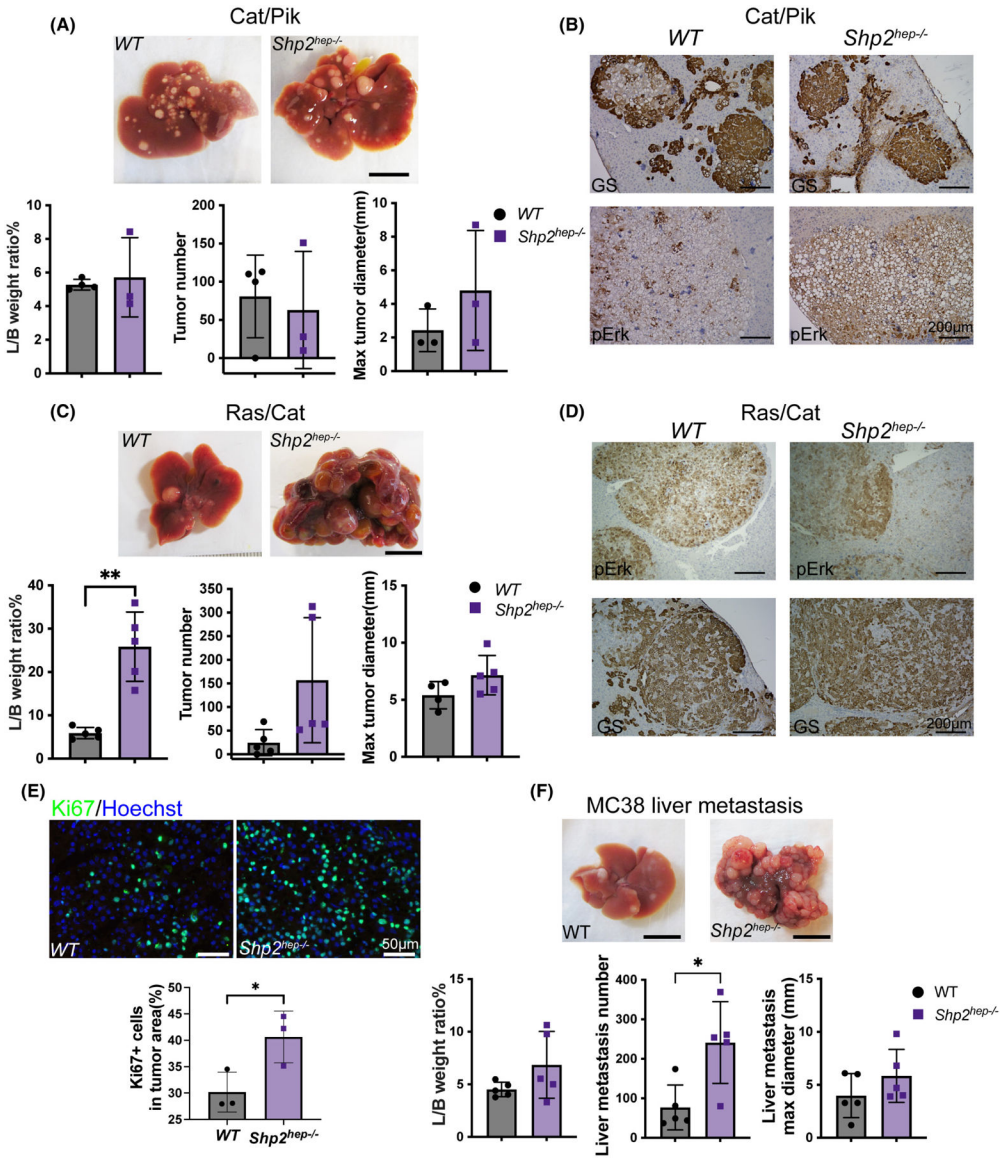

FIGURE 1.

Variable effects on liver tumor growth by genetic deletion of Shp2 in hepatocytes. (A) Representative macroscopic liver images, liver/body weight ratios, numbers, and maximal diameters of liver tumors induced by Cat/Pik in WT and *Shp2*$^{hep-/-}$ mice at Week 15 posttransfection. $n = 4$ (WT), 3 (*Shp2*$^{hep-/-}$). Scale bar, 1 cm. (B) Immunostaining of GS and pErk on Cat/Pik-transfected liver sections at 15 weeks posttransfection. (C) Representative macroscopic liver images, liver/body weight ratios, numbers, and maximal diameters of Ras/Cat-induced tumors in WT and *Shp2*$^{hep-/-}$ mice at Week 8 posttransfection. $n = 5$. Scale bar, 1 cm. (D) Immunostaining of pErk and GS on Ras/Cat-transfected liver sections. (E) Representative images and quantification of immunofluorescent staining of proliferative marker Ki67 in tumor area sections of Ras/Myc-driven liver. Four or more randomly selected microscopic fields of view were quantified for each biological sample. $n = 3$. (F) Representative macroscopic liver images, liver/body

weight ratios, numbers, and maximal diameters of metastasized tumors at 15 days post–intrasplenic transplantation of MC38 colon cancer cells (20,000 cells per mouse). $n = 5$. Scale bar, 1 cm. In (A,C,E,F), data are mean values ± SD, and p values were calculated by unpaired two-tailed Student t test. No annotation, not significant; *$p < 0.05$, **$p < 0.01$. L/B, liver/body.

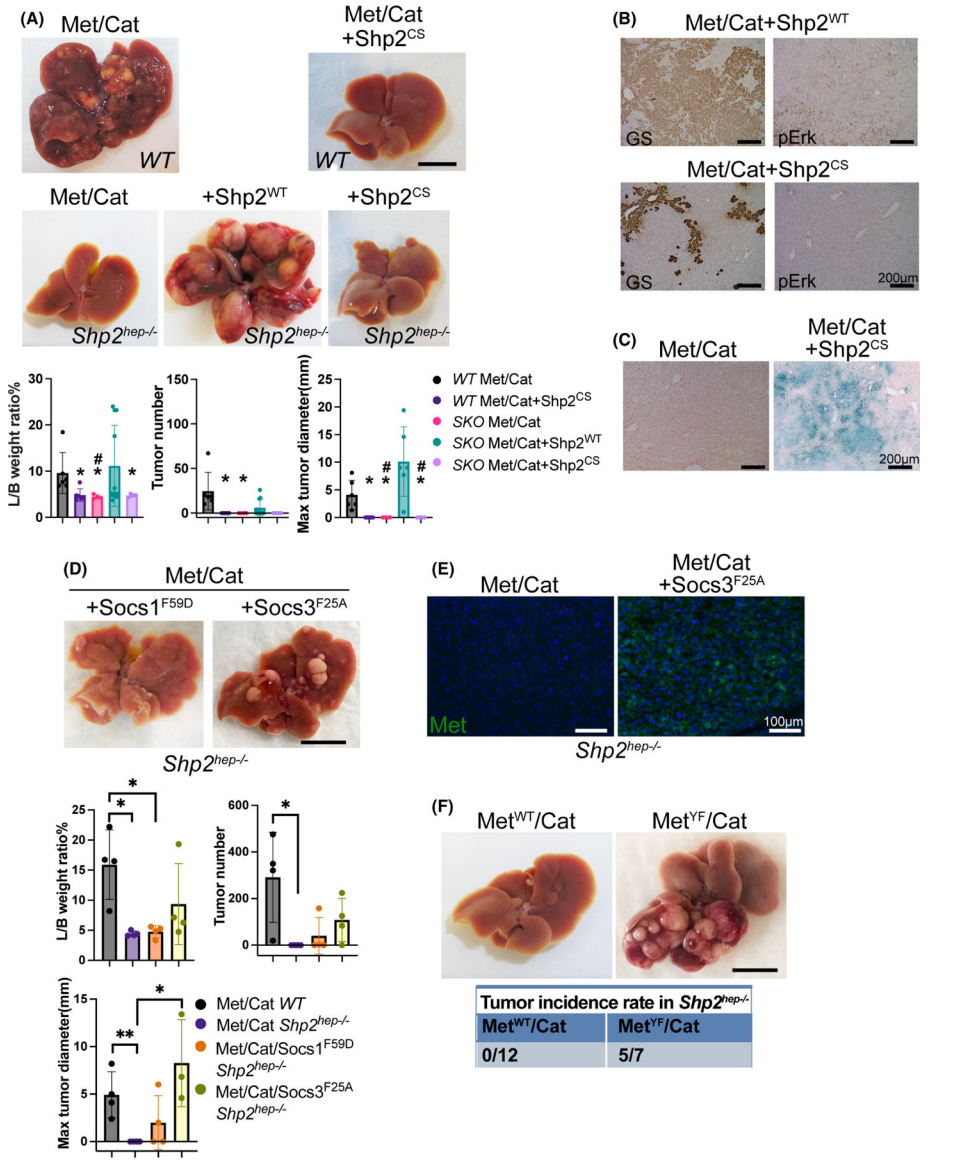

Tumor incidence rate in *Shp2*$^{hep-/-}$	
Met^{WT}/Cat	Met^{YF}/Cat
0/12	5/7

FIGURE 2.

The requirement of Shp2's catalytic activity for oncogenic signaling of RTK. (A) Representative macroscopic liver images, liver/body weight ratios, numbers, and maximal tumor diameters in WT or *Shp2*$^{hep-/-}$ (Shp2 knockout) livers following cotransfection of Met/Cat with WT Shp2^{WT} or catalytically inactive mutant Shp2^{CS}. n = 6 (WT Met/Cat), 6 (WT Met/Cat+Shp2^{CS}), 4 (Shp2 knockout Met/Cat), 11 (Shp2 knockout Met/Cat+Shp2^{WT}), 4 (Shp2 knockout Met/Cat+Shp2^{CS}). Scale bar, 1 cm. Symbols * and # indicate a significant difference between the annotated group versus WT Met/Cat group or versus the Shp2 knockout Met/Cat+Shp2^{WT} group, respectively. (B) Immunostaining of GS and pErk on sections of *Shp2*$^{hep-/-}$ liver transfected with Met/Cat plus WT or mutant Shp2. (C) Detection of cell senescence by β-galactosidase staining of WT liver sections transfected by Met/Cat, with or without Shp2^{CS} mutant. (D) Representative macroscopic images and physiological parameters of *Shp2*$^{hep-/-}$ livers transfected with Met/Cat+Socs1^{F59D} or Met/

Cat+Socs3^{F25A} at Week 10 posttransfection (tumorigenesis penetration ratio, 2/4 versus 3/4). $n = 4$. Scale bar, 1 cm. (E) Immunofluorescence staining of Met on Met/Cat or Met/Cat+Socs3^{F25A} transfected *Shp2*$^{hep-/-}$ livers at Week 8 posttransfection. (F) Representative macroscopic liver images and tumor incidence rates of *Shp2*$^{hep-/-}$ livers transfected with Met^{WT}/Cat or Met^{YF}/Cat. Scale bar, 1 cm. In (A,D), data are mean values ± SD, and p values were calculated by unpaired two-tailed Student t test. No annotation, not significant; $^{*,\#}p < 0.05$, $^{**,\#\#}p < 0.01$. L/B, liver/body; SKO, Shp2 knockout.

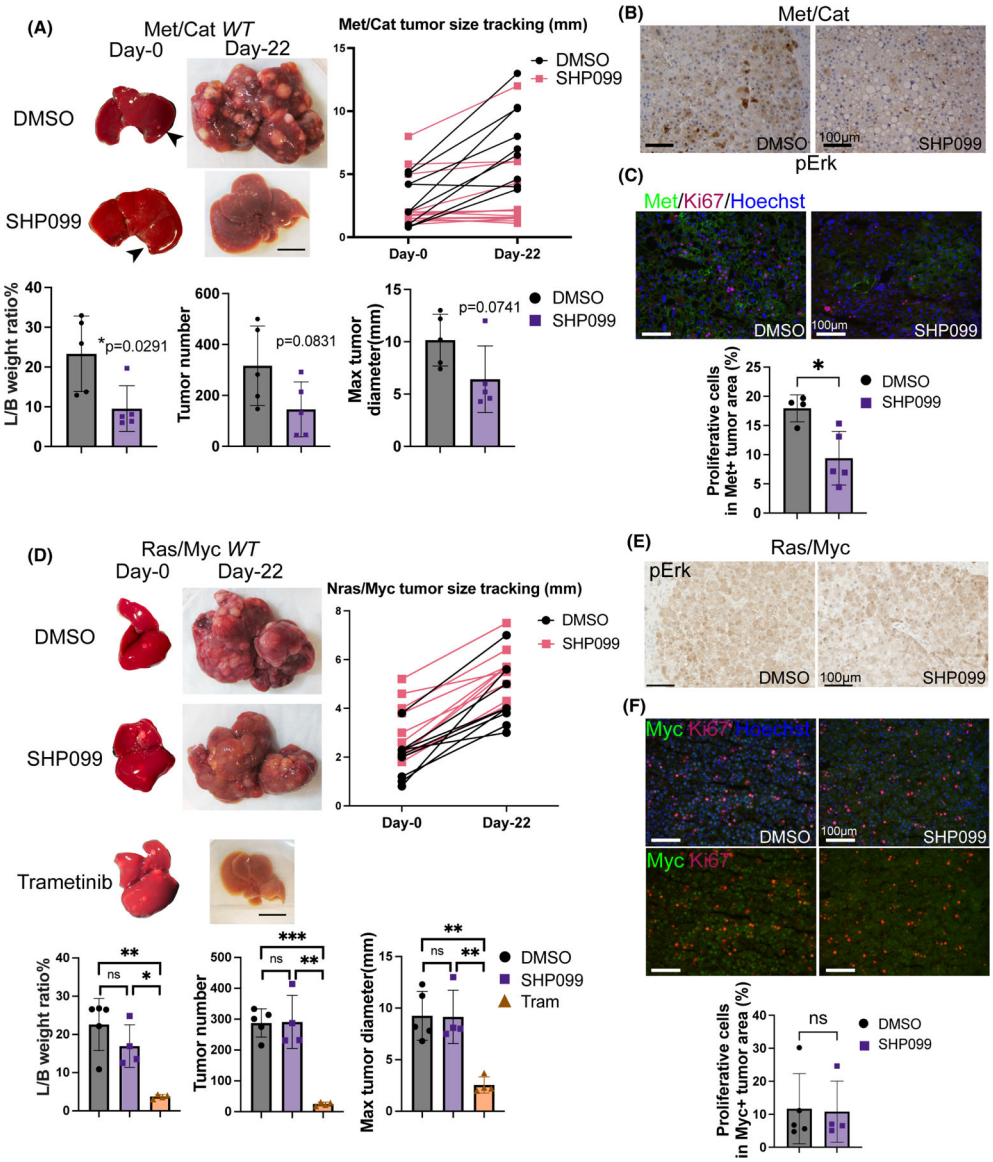

FIGURE 3.

Autochthonous liver tumor-inhibitory effects of SHP099. (A) Upper left: Representative macroscopic liver images before and after 3-week treatment with SHP099 or DMSO. Arrows point at established tumor nodules. Scale bar, 1 cm. Upper right: Size tracking of trackable tumor nodules. Lower: Quantitative analysis of liver/body weight ratios, tumor numbers, and sizes posttreatment. $n = 5$. (B) Immunostaining of pErk on Met/Cat tumor areas following DMSO or SHP099 treatment. (C) Immunofluorescence staining of Met and Ki67 on Met/Cat tumor areas following DMSO or SHP099 treatment, with quantification of $Ki67^+$ cell percentage in Met^+ tumor areas. Six randomly selected microscopic fields of view were quantified for each biological sample. $n = 4$ (DMSO), 5 (SHP099). (D) Upper left: Representative macroscopic liver images of Ras/Myc-transfected WT mice before and after 3-week treatment with DMSO, SHP099, or trametinib, which started when tumor sizes reached 2–3 mm. Upper right: Size tracking of trackable tumor nodules. Lower: Liver/body

weight ratio, tumor numbers, and sizes. $n = 5$ (DMSO), 4 (SHP099), 4 (trametinib). Scale bar, 1 cm. (E) Immunostaining of pErk on Ras/Myc-induced tumor areas following DMSO or SHP099 treatment in WT liver. (F) Immunofluorescent staining of Myc and Ki67 on Ras/Myc-induced tumor areas in WT liver following DMSO or SHP099, with quantification of $Ki67^+$ cell percentage in Myc^+ tumor areas. Six randomly selected microscopic fields of view were quantified for each biological sample. $n = 5$ (DMSO), 4 (SHP099). In (A,C,D,F), data are mean values ± SD, and p values were calculated by unpaired two-tailed Student t test. *$p < 0.05$, **$p < 0.01$, ***$p < 0.001$. L/B, liver/body; ns, not significant.

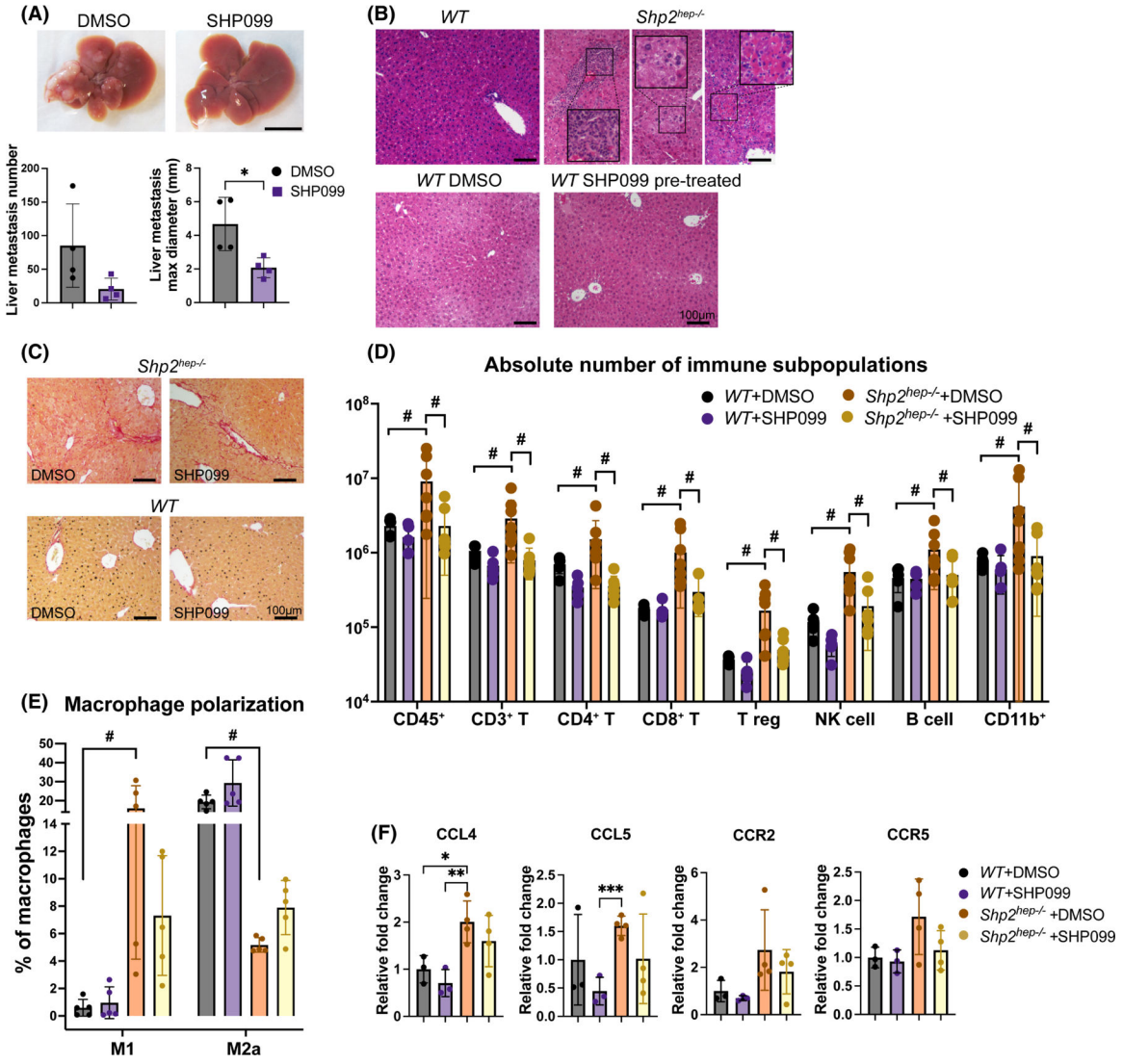

FIGURE 4.

Hepatic environmental effects caused by genetic versus pharmaceutical inactivation of Shp2. (A) Representative macroscopic images and liver metastasis measurements of DMSO-pretreated and SHP099-pretreated WT liver on Day 15 postinjection of MC38 cells (20,000 cells per mouse). $n = 4$. Scale bar, 1 cm. (B) Hematoxylin and eosin staining of untreated WT versus *Shp2*$^{hep-/-}$ liver and DMSO-pretreated versus SHP099-pretreated WT livers. Areas displaying infiltration of small-nucleus cells, ballooning hepatocytes, and necrotic tissue are highlighted and enlarged to show details. (C) Picrosirius red staining of DMSO/SHP099-pretreated *Shp2*$^{hep-/-}$ and WT liver. (D) Absolute cell numbers of major immune subsets in whole liver. (E) Percentages of polarized macrophages M1 (CD11c^{+} CD206^{-} F4/80^{+}) and M2a (CD11c^{-} CD206^{+} F4/80^{+}) of total macrophages in whole liver. (F) Quantitative RT-PCR measurements of CCL5–CCR5 axis–related gene transcript levels in isolated nonparenchymal cells from whole liver. Data are mean values ± SD. In (A,F), p values were calculated by unpaired two-tailed Student t test. No annotation, not significant; *$p < 0.05$, **$p < 0.01$, ***$p < 0.001$. In (D,E), p values were calculated by two-way

ANOVA together with multiple comparisons by the two-stage linear step-up procedure of Benjamini, Krieger, and Yekutieli. False discovery rate $q < 0.05$, $^{\#}p < 0.05$.

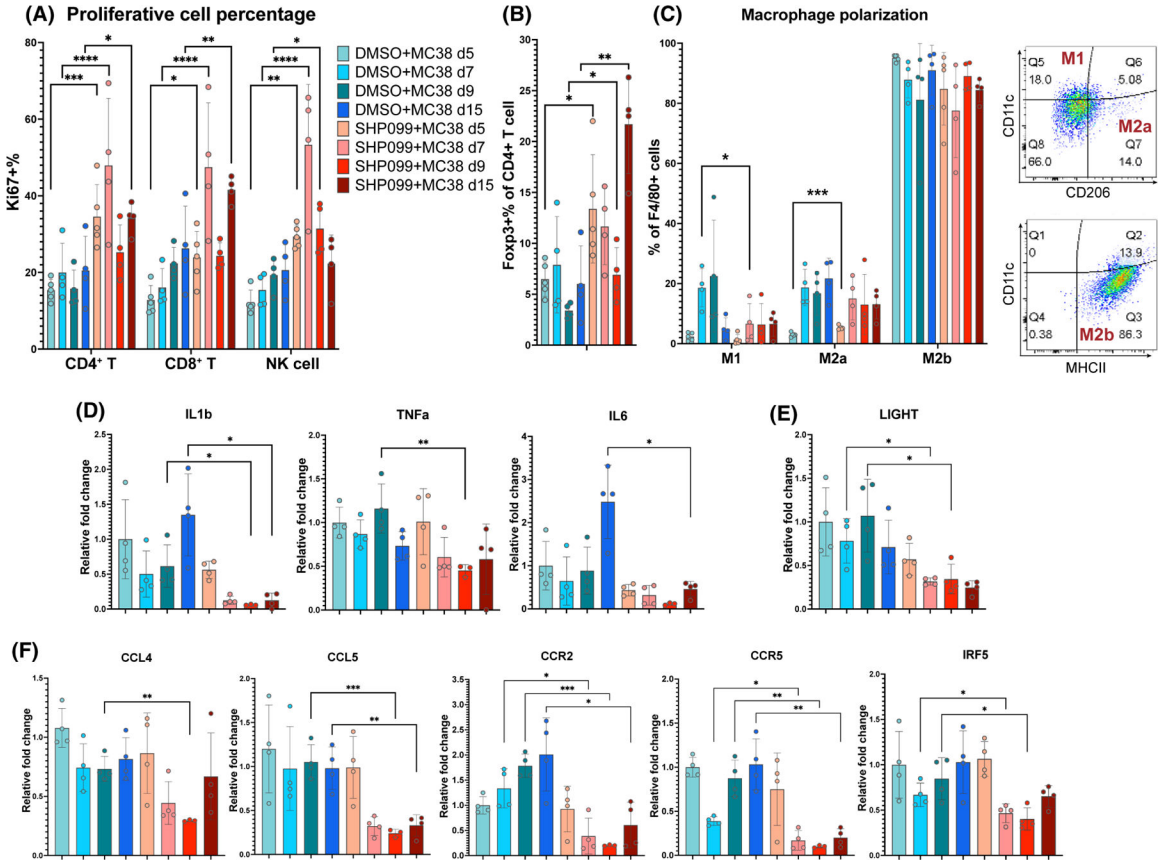

FIGURE 5.

Metastasized liver tumor-preventive effects of SHP099. (A) Percentages of Ki67$^+$ proliferative cells of T cell and NK cell subsets in whole WT liver. (B) Percentages of Treg cells (forkhead box P3–positive CD4$^+$) in total CD4$^+$ T cells in whole WT liver. (C) Left: Percentages of polarized macrophages M1 (CD11c$^+$ CD206$^-$ F4/80$^+$), M2a (CD11c$^-$ CD206$^+$ F4/80$^+$), and M2b (CD11c$^-$ MHCII$^+$ F4/80$^+$) in total macrophages in whole WT liver. Right: Representative FACS plots gated on macrophages showing separation of three polarized subsets. (D–F) Quantitative RT-PCR measurement of mRNA levels for (D) proinflammatory factors, (E) LIGHT/TNFSF14, and (F) CCL5–CCR5 axis–related genes in isolated nonparenchymal cells from whole WT liver. Data are mean values ± SD, and *p* values were calculated by unpaired two-tailed Student *t* test. No annotation, not significant; *$p < 0.05$, **$p < 0.01$, ***$p < 0.001$. Foxp3, forkhead box P3.

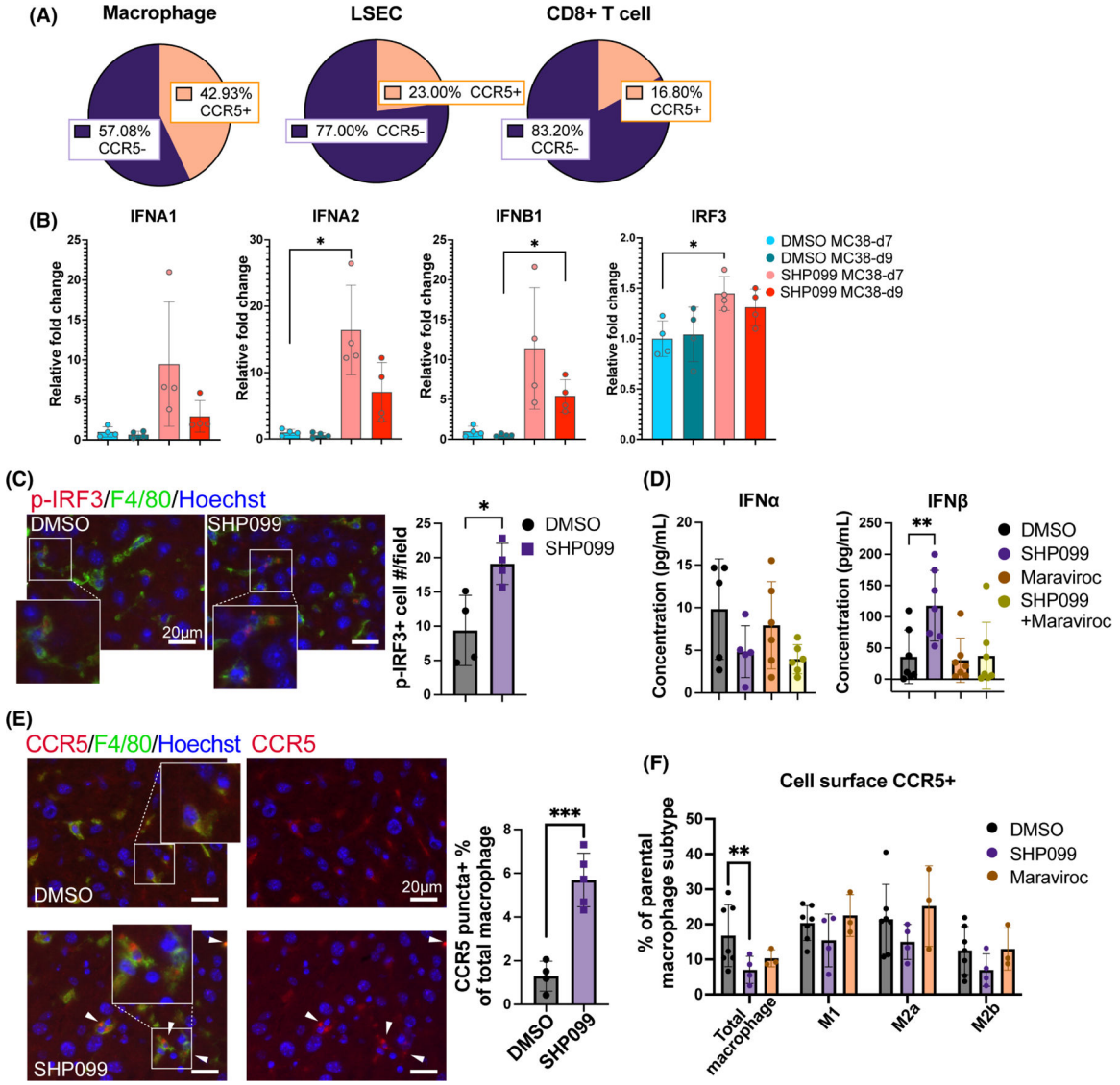

FIGURE 6.

Effects of SHP099 on IFN signaling induction and CCR5 suppression. (A) Top three ranked nonparenchymal cell subsets with largest CCR5$^+$ portion in WT liver on Day 7 post–MC38 transplantation. (B) Quantitative RT-PCR measurements of mRNA levels of Type I IFNs and IRF3 in isolated nonparenchymal cells from pretreated WT liver. (C) Immunofluorescent staining of p-IRF3 and F4/80 in pretreated WT liver on Day 7 post–MC38 transplantation. p-IRF3$^+$ cells were quantified based on six randomly selected microscopic fields of view for each biological sample. $n = 4$. (D) ELISA measurement of secreted IFNα and IFNβ in supernatants of isolated liver macrophages cultured with the indicated inhibitors for 16 h. (E) Immunofluorescence staining of CCR5 (arrows, punctate CCR5 expression) and F4/80 in pretreated WT liver on Day 9 post–MC38 transplantation. Punctate CCR5$^+$ F4/80$^+$ cells were quantified based on six randomly selected microscopic fields of view for each biological sample. $n = 4$ (DMSO), 5 (SHP099). (F) Cell surface CCR5$^+$ cell percentage in each polarized macrophage subset or total macrophage. Data are mean values ± SD, and

p values were calculated by unpaired two-tailed Student *t* test in (B,C,E,F) or by paired two-tailed Student *t* test in (D). No annotation, not significant; **p* < 0.05, ***p* < 0.01, ****p* < 0.001.

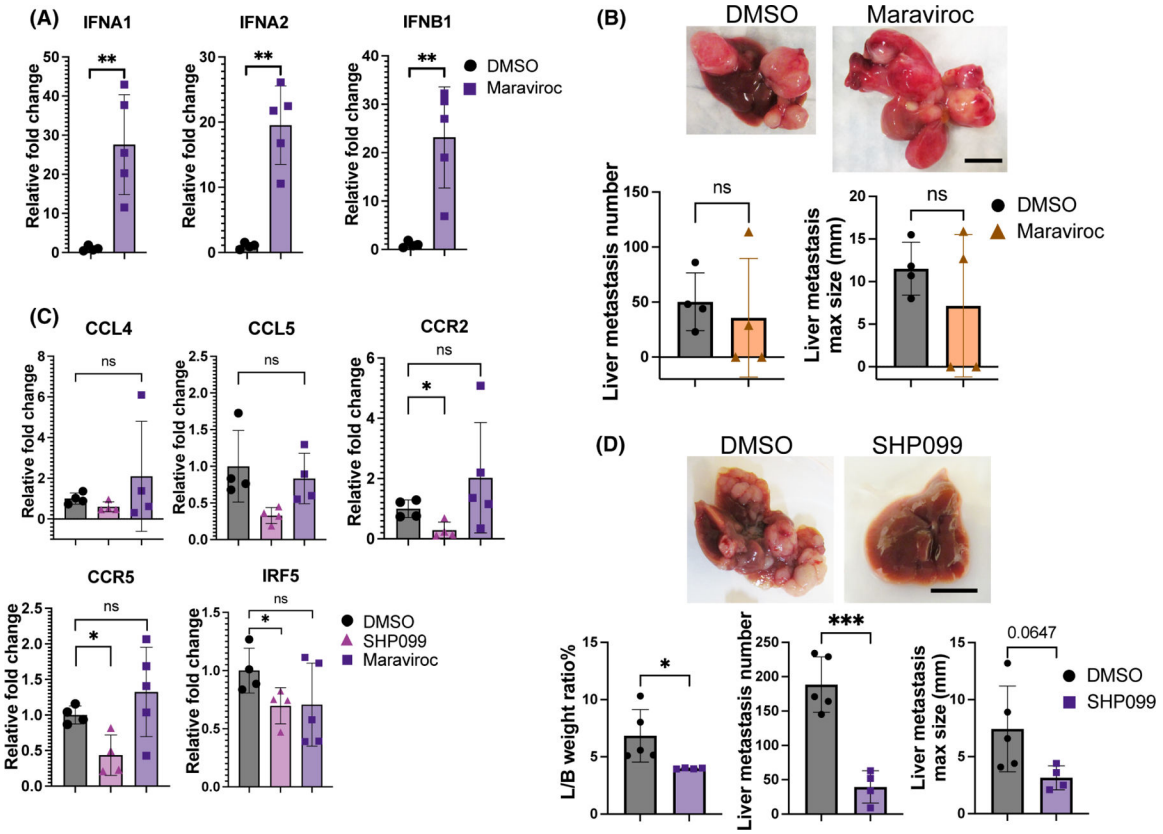

FIGURE 7.

Hepatic antitumor effects mediated by SHP099 versus Maraviroc. (A) Quantitative RT-PCR measurement of mRNA levels of IFNA1, IFNA2, and IFNB1 in nonparenchymal cells isolated from treated WT liver on Day 7 post–MC38 transplantation. (B) Representative macroscopic images and quantification of metastasized tumors in WT livers treated with DMSO or Maraviroc. Experiments were terminated on Day 25 post–intrasplenic MC38 transplantation (7000 cells per mouse). $n = 4$. Scale bar, 1 cm. (C) Quantitative RT-PCR measurements of mRNA levels of CCL5–CCR5 axis–related genes in isolated nonparenchymal cells from treated WT liver on Day 7 post–MC38 transplantation. (D) Representative macroscopic images and quantification of metastasized tumor in WT livers under DMSO or SHP099 treatment that started after MC38 splenic transplantation. $n = 5$ (DMSO), 4 (SHP099). Scale bar, 1 cm. Data are mean values ± SD, and p values were calculated by unpaired two-tailed Student t test. No annotation, not significant; *$p < 0.05$, **$p < 0.01$, ***$p < 0.001$. L/B, liver/body; ns, not significant.